Journal of Advanced Research 53 (2023) 249–260

Contents lists available at ScienceDirect

Journal of Advanced Research

journal homepage: www.elsevier.com/locate/jare

Original Article

# Antisense-oligonucleotide co-micelles with tumor targeting peptides elicit therapeutic effects by inhibiting microRNA-21 in the glioblastoma animal models

Youngki Lee [1], Junkyu Ha [1], Minkyung Kim, Subin Kang, Minji Kang, Minhyung Lee *

*Department of Bioengineering, College of Engineering, Hanyang University, Seoul 04763, South Korea*

## HIGHLIGHTS

- Co-micelles were produced with cholesterol-conjugated anti-microRNA-21 oligonucleotides (AMO21c) and cholesterol-conjugated T7 peptides (T7c).
- Co-micelles with AMO21c and T7c delivered AMO21c efficiently into the brain by intranasal administration.
- Intranasal administration of the co-micelles elicited anti-tumor effect in intracranial glioblastoma models.

## GRAPHICAL ABSTRACT

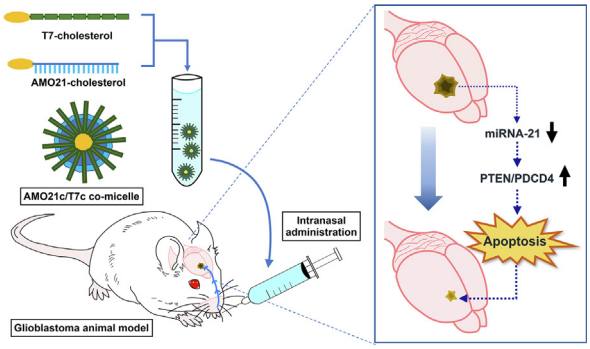


## ARTICLE INFO

*Article history:*
Received 23 September 2022
Revised 14 November 2022
Accepted 7 January 2023
Available online 9 January 2023

*Keywords:*
Antagomir
Glioblastoma
Intranasal delivery
Micelle
miRNA

## ABSTRACT

*Introduction:* miRNA-21 (miR-21) is highly expressed in glioblastoma, facilitating tumor growth by blocking the expression of apoptosis-related genes. Therefore, an antisense microRNA oligonucleotide (AMO) against miR-21 was suggested as a therapeutic nucleic acid for glioblastoma.
*Objectives:* AMO21 co-micelles were developed with tumor-targeting T7 peptides as an AMO21 delivery system by intranasal administration.
*Methods:* Cholesterol-conjugated AMO21 (AMO21c) was mixed with cholesterol-conjugated T7 peptides (T7c) to produce tumor-targeted co-micelles. Physical characterization was performed by dynamic light scattering, gel retardation assay, scanning electron microscope and heparin competition assay. *In vitro* transfection efficiency to C6 glioblastoma cells was measured by flow cytometry. The AMO21c/T7c co-micelles were administered by intranasal instillation into the brain of intracranial glioblastoma rat models. Scrambled T7 (scrT7) and scrambled AMO21c (scrAMO21c) were used as a negative control. The therapeutic effects of the AMO21c/T7c co-micelles were evaluated by real time RT-PCR, immunohistochemistry, TUNEL assay, and Nissl staining.
*Results:* The formation of the AMO21c/T7c co-micelles was confirmed in gel retardation and heparin competition assays. The highest delivery efficiency *in vitro* was achieved at a 1:10 wt ratio of AMO21c/T7c. The AMO21c/T7c co-micelles had higher delivery efficiency into C6 glioblastoma cells than naked AMO21c or AMO21c/lipofectamine complexes. After intranasal administration into the intracranial glioblastoma models, the delivery efficiency of the co-micelles into the brain was also higher than those of naked AMO21c and AMO21c/scrambled T7c. Thanks to their enhanced delivery efficiency, the AMO21c/T7c co-micelles downregulated miR-21, inducing the production of the pro-apoptotic

Peer review under responsibility of Cairo University.
* Corresponding author.
*E-mail address:* minhyung@hanyang.ac.kr (M. Lee).
[1] Co-first authors: These authors contributed equally.

https://doi.org/10.1016/j.jare.2023.01.005

phosphatase and tensin homolog (PTEN) and programmed cell death 4 (PDCD4) proteins in the tumor tissues. The tumor size was reduced by the AMO21c/T7c co-micelles more effectively than naked AMO21c, AMO21c/lipofectamine, or scrAMO21c/T7c treatment.

*Conclusion:* The results suggest that the co-micelles of AMO21c and T7c may be an efficient delivery system into a brain tumor through intranasal administration.



## Introduction

Glioblastoma multiforme is a critical disease with an average survival of <5 years after diagnosis [1]. The therapeutic options are surgery and chemo- and radiotherapy [2]. Although progress has been made for glioblastoma therapy, the currently available treatments have limitations. Because aggressive surgery is not appropriate in the brain, complete resection is almost impossible. Furthermore, tumor cells frequently migrate in the brain, which aggravates the recurrence of glioblastoma after surgery [2]. Chemo- and radiotherapy also have problems, such as side-effects on normal cells and frequent recurrence. Therefore, new therapeutic modalities to treat glioblastoma have been suggested and are being investigated.

One of those new approaches is gene therapy [3–6], which uses therapeutic nucleic acids and their carriers. Therapeutic nucleic acids include genes that induce cell death, such as the HSV thymidine kinase gene [7]. Genes need to be expressed into proteins in the tumors to have their therapeutic effects. For this purpose, the genes must be delivered into the nuclei of the tumor cells for transcription. Small nucleic acids such as antisense oligonucleotides are another type of therapeutic nucleic acid [8,9]. These nucleic acids do not require delivery into cell nuclei to have therapeutic effects. In the cytoplasm, they interact with their target RNAs and facilitate their degradation, producing therapeutic effects. The VEGF siRNA, which inhibits tumor angiogenesis, is a representative example of this type [10]. Recently, antisense oligonucleotides against microRNAs (miRNA) have been investigated as therapeutic nucleic acids [5,11–14]. Many reports have shown that some miRNAs in tumors have oncogenic effects and are involved in the pathogenesis of a tumor [5,15,16]. They are usually overexpressed in tumor cells. As a result, they inhibit the expression of genes related to tumor suppression and apoptosis. For example, miRNA-21 (miR-21) is highly expressed in malignant human glioblastoma tissues, facilitating tumor growth as a key anti-apoptotic factor by blocking the expression of apoptosis-related genes such as phosphatase and tensin homolog (PTEN) and down-regulating programmed cell death 4 (PDCD4) [5,17–19]. Therefore, an anti-miRNA oligonucleotide (AMO), which is also called an 'antagomir,' could have therapeutic effects by inhibiting oncogenic miRNAs [15]. In the case of miR-21, the delivered AMO against miR-21 (AMO21) can induce the high gene expression levels of PDCD4 and PTEN in cancer cells. In previous studies, the AMO21 proved its therapeutic efficiency by successfully inhibiting miR-21 and decreasing glioblastoma tumor size in vivo [9,13,20–22].

Another component of gene therapy is the carriers used to deliver the therapeutic nucleic acids. Safe and efficient carriers are needed to maximize the therapeutic effects of AMOs. Various AMO carriers have been developed for glioblastoma therapy, including cationic polymers, peptides, and exosomes [6,23–26]. Deoxycholate-conjugated polyethylenimine (DA-PEI) was evaluated as a carrier of AMO21 for glioblastoma therapy [22]. In the previous study, curcumin-loaded DA-PEI (DA-PEI/Cur) formed complexes with AMO21, and those complexes were then injected locally into brain tumors using stereotaxic equipment. As a result, DA-PEI/Cur delivered AMO21 into the tumor cells more efficiently than naked AMO21 and produced reductions in tumor size. For a local injection, R3V6 amphiphilic peptides were evaluated as an AMO21 carrier for the treatment of glioblastoma [21]. To test the feasibility of targeted AMO21 delivery with systemic administration in an intracranial glioblastoma model, T7 peptide-decorated exosomes (T7-exo) were developed as an AMO21 carrier and given by tail-vein injection [13]. The T7-exo facilitated the delivery of AMO21 into the tumors, compared with naked AMO21 and unmodified exosomes. For brain-tumor targeted delivery by intranasal delivery, a cationic peptide, RAGE-binding peptide (RBP), was used as an AMO21 carrier [20]. After intranasal administration of the RBP/AMO21 complex, AMO21 was effectively delivered into the glioblastoma tissues, and tumor size decreased.

The carriers just described all had a higher delivery efficiency than naked AMO21. However, they are not free of side-effects. For example, cationic polymers and peptides can induce cytotoxicity. It was previously reported that positively charged polymer/DNA complexes interact with cell membranes, inducing aggregation and rupture on cell surfaces [27]. Exosomes also have side-effects because their contents (miRNAs, mRNAs, proteins, or DNA) are not controllable. Therefore, minimal usage of carriers could be beneficial.

Cholesterol-conjugated materials can form a micelle structure in an aqueous solution and be used to deliver nucleic acids. For instance, cholesterol-conjugated polymers were used to form a micelle structure and deliver plasmid DNA [28–30]. In other studies, cholesterol was conjugated to siRNAs to form micelles in an aqueous solution and increase the delivery efficiency of siRNAs [31]. Therefore, conjugating cholesterol to AMOs could induce the formation of a micelle structure. In this study, cholesterol was conjugated to the 3′-end of AMOs to form micelles in an aqueous solution.

In this study, cholesterol-conjugated AMOs were intranasally administered to rats, and their arrival in glioblastomas was evaluated. Intranasal administration has been suggested as an efficient strategy for delivering therapeutics into the brain [32,33]. It has shown particular efficiency against glioblastoma [34]. Intranasal administration has some qualities, compared with local injection and intravenous (IV) injection. First, the procedure is less invasive, compared with local or IV injection. Surgery to the brain often carries critical risks to patients. Due to the irreplaceable role of the brain, tissue damage to neurons during stereotaxic injection can crucially affect quality of life. Therefore, a less invasive procedure could be beneficial for glioblastoma patients. Second, the delivery efficiency of intranasal administration is higher than that of IV injection. Although brain-targeting carriers have been developed, most of the drugs are taken up by the liver after an intravenous injection. On the other hand, intranasal administration delivers nanoparticles through olfactory and trigeminal pathways that reduce the chance that they will be eliminated. Third, intranasal administration can preserve micelles better than an intravenous injection. As shown in another study, the hydraulic pressure of blood can destabilize the micelle structure by up to 80% [35]. Most nanoparticles might thus be degraded before they reach the brain if they are delivered intravenously because only extremely stable micelles with a low critical micelle concentration (CMC) can

endure blood pressure [36–38]. However, intranasal administration might not have those disadvantages, which could increase delivery efficiency into the brain.

In this study, the T7 peptide (HAIYPRH) was used for targeting delivery as a targeting ligand [39]. The T7 peptide binds to the transferrin receptor (TfR). TfR is involved in the cellular uptake of iron from transferrin by means of endocytosis. Previous reports showed that TfR is highly overexpressed on both malignant tumor cells and brain capillary endothelial cells, compared with normal cells [40]. The T7 peptide is a ligand specific for TfR. In this study, cholesterol-conjugated T7 peptide (T7c) and AMO21c were mixed to produce tumor-targeted co-micelles. The co-micelles of AMO21c and T7c were characterized physically, and the delivery efficiency of the co-micelles was evaluated *in vitro*. In an intracranial glioblastoma model, the AMO21c/T7c co-micelles were administered intranasally, and their anti-tumor effects were evaluated by various methods. The results suggest that the AMO21c/T7c co-micelles could be useful for delivering AMO21 into glioblastoma.

## Materials & methods

### *Materials*

DMEM, FBS, and DPBS were obtained from Welgene (Daegu, Korea). C6 rat glioblastoma cells were purchased from the Korean Cell Line Bank (Seoul, Korea). MTT and heparin were obtained from Pierce (Waltham, MA). T7 peptide (T7, HAIYPRH), T7c (cholesterol-HAIYPRH), and scrambled T7c (scrT7c, cholesterol-IRHPHYA) were synthesized by Peptron (Daejeon, Korea). AMO21c (5′-UCAACAUCAGUCUGAUAAGCUA-3′), scrAMO21c (5′-CAUUAAUGUCGGACAACUCAAU-3′), GAPDH primers, and miRNA-21 primers were synthesized by Bioneer (Daejeon, Korea). Cholesterols of AMO21c and scrAMO21c were conjugated at the 3′-end of the oligonucleotides. A SensiFAST SYBR No-ROX kit was obtained from Bioline (Boston, MA). Rabbit PDCD4 antibodies were obtained from Bethyl Laboratories (Montgomery, TX). Fluorescence mounting medium was obtained from DAKO (Carpinteria, CA). Mouse PTEN antibodies were provided by Santa Cruz Biotechnology (Dallas, TX). Goat anti-mouse IgG and goat anti-rabbit IgG with Alex Fluor 488 were obtained from Invitrogen (Carlsbad, CA). Ki-67 monoclonal antibodies were provided by Enzo Life Sciences (Farmingdale, NY). Deparaffinization solution and an miRNeasy FFPE kit were purchased from Qiagen (Valencia, CA). A Label IT nucleic acid labeling kit with Cy5 was obtained from Mirus Bio (Madison, WI). An iScript cDNA synthesis kit was purchased from Bio-Rad (Hercules, CA). TUNEL assay kit was provided by Abcam (Cambridge, MA).

### *Transfection and flow cytometry assay*

C6 glioblastoma cells were maintained in DMEM with 10% FBS. For transfection assays, the cells were seeded in a 12-well microassay plate at $2 \times 10^5$ cells/well. After 24 h of incubation, the culture media were replaced with serum-free media. The AMO21 was labeled with cyanine 5 (Cy5) with the Label IT nucleic acid labeling kit. To optimize the weight ratio, the Cy5-labeled AMO21c (Cy5-AMO21c)/T7c co-micelles were prepared at different weight ratios. The preparation of the AMO21c/T7c co-micelles were performed by simply mixing two components. The co-micelles were formed spontaneously in the aqueous solution.

The AMO21c/T7c co-micelles (0.2 μg Cy-AMO21c/well) were then added to C6 cells. For the addition of the micelles, the cells were incubated at 37℃ for 4 h. The transfected cells were harvested by centrifugation at 500*g* for 3 min, followed by washing by PBS. After resuspension of the cells in PBS, flow cytometry was carried out to evaluate transfection efficiency using a BD FACS Calibur (BD Biosciences, San Jose, CA).

For the comparison of transfection efficiency, the Cy5-AMO21c/T7c co-micelles were produced at a weight ratio of 1:10. Cy5-AMO21c/lipofectamine complexes at a 1:3 ratio (w/w) and naked Cy5-AMO21c were used as controls. Transfection and the flow cytometry assay were performed as described above.

### *Gel retardation assay*

The production of the AMO21c/T7c co-micelles was confirmed by a gel retardation assay. The amount of AMO21c was fixed at 0.5 μg per well. Lipofectamine, T7c, and T7 were added to the AMO21c solution at various weight ratios. After 30 min of incubation, the mixtures were subjected to electrophoresis on a 2% agarose gel.

### *Heparin competition assay*

AMO21c/T7c co-micelles were prepared at a 1:10 wt ratio. AMO21c/lipofectamine complexes at a 1:3 (w/v) ratio were used as a control. After 30 min of incubation, heparin was mixed to the samples at various doses. The samples were incubated for additional 30 min. Then, the samples were analyzed by agarose gel electrophoresis.

### *Scanning electron microscopy (SEM)*

AMO21c/T7c co-micelles were produced at a weight ratio of 1:10. The co-micelles were mounted and dried on a grid. Then the mounted co-micelles were covered with Pt. The co-micelles were investigated by SEM (FEI, Hillsboro, OR).

### *Dynamic light scattering*

AMO21c/T7c co-micelles and lipofectamine/AMO21c complexes were produced at various ratios. The samples were maintained at room temperature for 30 min. Then the zeta-potential and hydrodynamic size of the complexes were investigated using a Zetasizer Nano ZS system (Malvern Instruments, Malvern, UK).

### *Measurement of CMC*

AMO21c, T7c, and AMO21c/T7c co-micelles (a 1:10 wt ratio) were produced at various concentrations. One microgram of DPH was mixed with the samples, which were then incubated at room temperature for 4 h. After the incubation, the DPH excitation and emission wavelengths were measured at 355 nm and 428 nm, respectively. The CMC values were measured using a microplate reader (Tecan, Switzerland) and analyzed by nonlinear regression.

### *MTT assay*

C6 cells were seeded in a 96-well microassay plate at $1 \times 10^4$ cells/well and maintained at 37 ℃ for 24 h. Prior to transfection, the culture medium was changed to serum-free medium. To exclude the induction of apoptosis by AMO21c, scrambled AMO21c (scrAMO21c)/T7c micelles were produced with scrAMO21c at various weight ratios and used for the cytotoxicity assays. ScrAMO21c/lipofectamine complexes at a 1:3 wt ratio were used as a control. MTT assay was performed as described previously [20,41].

### *Fluorescence microscopy study*

C6 cells were seeded on a chamber slide at $1 \times 10^5$ cells/well. Cy5-AMO21c/T7c co-micelles and AMO21c/lipofectamine com-

plexes were produced and transfected to the cells. After transfection, the cells were washed twice with DPBS. The nuclei were stained with DAPI. The slides were investigated with an AxioScan slide scanner (ZEISS, Oberkochen, Germany).

*Ethics statement*

Animal experiment protocols were approved by the Institutional Animal Care and Use Committee (IACUC) of Hanyang University (accreditation number: 2019–0205). All animal experiments followed the guidelines of the IACUC.

*Intracranial glioblastoma animal model*

The intracranial glioblastoma models were established with seven-week-old male Sprague Dawley rats as described previously [13,20]. The rats were divided randomly into 5 groups: control, naked AMO21c, AMO21c/lipofectamine, AMO21c/T7c, and scrAMO21c/T7c. One-week after the transplantation, the samples were administrated daily into the rats using a pressurized olfactory device (POD) (Impel NeuroPhrama, Seattle, WA) for three consecutive days [42]. The injection samples were produced at optimal ratios for transfection. The amount of AMO21c was 1 μg/administration and the volume of the samples was 30 μl/administration. Normal saline was administered as a negative control. A week after the first intranasal administration, the rats were sacrificed and the brains were harvested. The brains were fixed with 4% paraformaldehyde.

*Nissl staining*

The paraffin embedded brain samples were cut into 10-μm thick sections. The sections were put on a slide glass and stained with cresyl violet. The stained samples were analyzed using ImageJ software.

*Quantitative RT-PCR*

Quantitative RT-PCR was performed as described previously [20]. The sequences of the primers were as follows: GAPDH forward primer, 5′-AGA CAG CCG CAT CTT CTT GT-3′; GAPDH backward primer, 5′-CTT GCC GTG GGT AGA GTC AT- 3′; miR-21 forward primer, 5′-GCC CGC TAG CTT ATC AGA CTG ATG-3′; miR-21 backward primer, 5′-GTG CAG GGT CCG AGG T- 3′.

*Immunohistochemistry*

The paraffin embedded brain samples were cut into 6-μm sections. The immunohistochemistry was carried out with anti-PDCD4 antibodies, anti-PTEN antibodies, and anti-Ki-67 antibodies as described previously [20].

*TUNEL assay*

The paraffin embedded brains were cut into 6-μm sections. TUNEL assay was performed as described previously [20]. The samples were analyzed using AxioScan slide scanner (ZEISS, Oberkochen, Germany).

*Evaluation of in vivo delivery efficiency using Cy5.5-labeled AMO21c*

AMO21c was labeled with Cy5.5 using a Label IT labeling kit. The Cy5.5-AMO21c/T7c co-micelles and Cy5.5-AMO21c/scrT7c complexes were produced in saline at optimal ratios. Two weeks after the animals received the injection of C6 cells, the samples were administered intranasally using POD. Normal saline was administered to the control animals. The total administered volume was 60 μl (30 μl/nostril). The amount of Cy5.5-AMO21c was 10 μg per animal. Two hours after the administration, the brains were harvested and observed with the FOBI imaging system (Neo Science, Suwon, Korea).

*Statistical analysis*

All data in this study are presented as the means ± standard deviations. Statistical analysis was performed using ANOVA. P-values<0.05 were considered statistically significant.

## Results and discussion

*Characterization of the AMO21c/T7c co-micelles*

To efficiently deliver AMO21 into the brain, cholesterol was conjugated to AMO21 to produce AMO21c micelles. To ensure tumor-specific binding, T7c was mixed with AMO21c to produce AMO21c/T7c co-micelles (Fig. 1). The AMO21c/T7c co-micelles were administered to the orthotopic glioblastoma model animals by intranasal instillation to allow them to enter the brain directly through trigeminal and olfactory pathways, which bypass the blood–brain barrier. In addition, intranasal administration might allow the AMO21c/T7c to interact with serum proteins and cells in the blood less than they would with intravenous administration, which could increase delivery efficiency to the brain.

To determine the optimum ratio of AMO21c and T7c, *in vitro* delivery efficiency was measured by transfecting C6 cells with the AMO21c/T7c co-micelles. Compared with the AMO21c micelles, the AMO21c/T7c co-micelles had a tendency toward increased efficiency as the ratio of T7c increased (Fig. 2). The delivery efficiency began to plateau around a 1:10 wt ratio. The efficiency gaps at the tested ratios (1:5–1:10 and 1:10–1:20) decreased dramatically around 1:10 (Fig. 2). In addition, the efficiency at 1:10 did not differ significantly from that at 1:20 or 1:30. Therefore, the weight ratio between AMO21c and T7c was fixed at 1:10 for the following experiments.

Physical characterization of the AMO21c/T7c co-micelles was performed using various assays. Gel retardation assays were carried out to verify micelle formation. In general, gel retardation assays have been used to identify complexes that form between nucleic acids and cationic polymers by means of charge interactions. Because the cationic polymers neutralize the charge of the nucleic acids, the complexes lose their mobility in the gels. T7 peptides have cationic characteristics. The amino acid sequence of the T7 peptide is HAIYPRH, which indicates that it has a + 1 charge at neutral pH. A charge interaction between AMO21c and T7c might thus contribute to complex formation. However, the gel retardation assay showed that AMO21c was not retarded (Fig. 3A), indicating that it might not be neutralized by the T7 peptide. On the other hand, in the mixture of AMO21c and T7c, AMO21c was retarded completely at a AMO21c/T7c weight ratio of 1:5 (Fig. 3A). This result suggests that T7c might have an additional interaction with AMO21c, compared with T7, and that the additional interaction could be hydrophobic due to the cholesterol moieties. Lipofectamine retarded AMO21c completely at a 1:3 wt ratio (Fig. 3A). Because the retardation of DNA or RNA in a gel retardation assay is usually due to a charge interaction, AMO21c might also be retarded mainly by a charge interaction. However, lipofectamine could also have a hydrophobic interaction with AMO21c.

The physical stability of the micelles was evaluated using heparin competition assays (Fig. 3B). The AMO21c/lipofectamine complexes released AMO21c by the addition of 3 μg of heparin. The AMO21c/T7c co-micelles began to release AMO21c by the addition

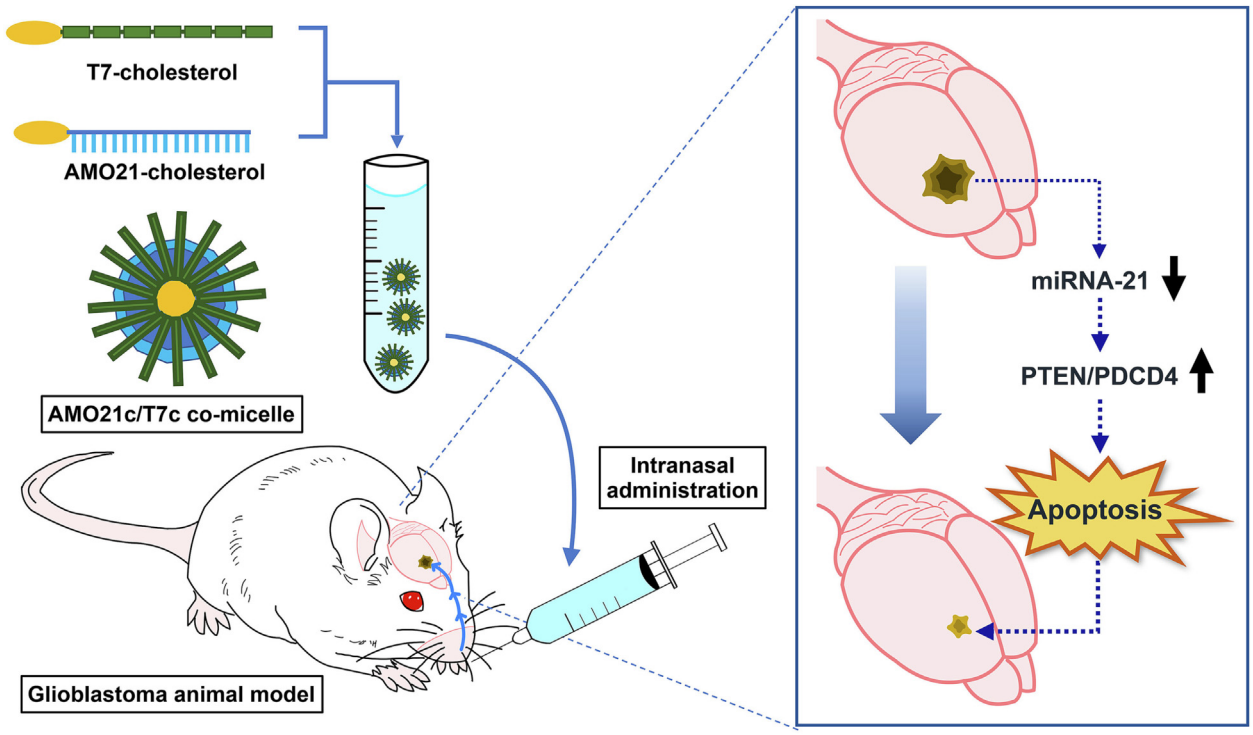


**Fig. 1.** Schematic representation of the AMO21c/T7c co-micelles.

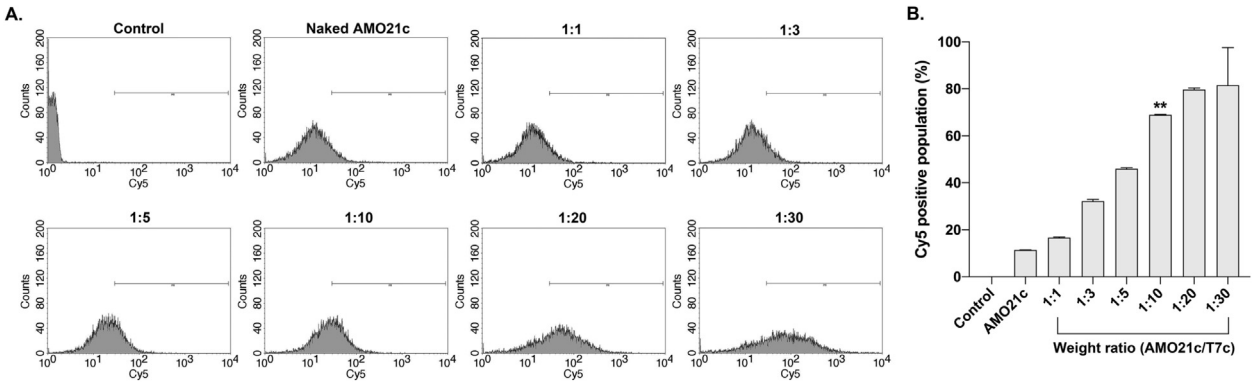


**Fig. 2. Delivery efficiency of the AMO21c/T7c co-micelles, depending on the weight ratio.** Cy5-AMO21c/T7c co-micelles at various weight ratios were transfected into C6 cells. Flow cytometry was performed to evaluated the delivery efficiency. **(A) Fluorescence intensity histograms of flowcytometry and (B) Mean values of intracellular uptakes.** The data are expressed as the mean ± standard deviation of triplicate experiments. **P < 0.01 compared with all the other samples except 1:20 and 1:30.

of 1 μg of heparin. However, most of the AMO21c was not released from the micelles even in the presence of 10 μg of heparin (Fig. 3B). Nucleic acid/cationic carrier complexes can release nucleic acids due to disruption of the charge interaction caused by heparin. In the heparin competition assays, the AMO21c/lipofectamine complex released AMO21c in the presence of excess heparin, suggesting that the interaction between AMO21c and lipofectamine could be mainly a charge interaction. On the contrary, most of the AMO21c in the AMO21c/T7c co-micelles were not released in the presence of excess heparin, indicating that a hydrophobic interaction could contribute significantly to the formation of the AMO21c and T7c micelles.

The SEM analysis indicated that the AMO21c/T7c co-micelles had a spherical shape (Fig. 3C). Their zeta potential and particle size of the micelles were measured by dynamic light scattering (Fig. 3D and 3E). The sizes at weight ratios of 1:5 and 1:10 were 164.43 ± 4.1 nm and 171.56 ± 0.8 nm, respectively, whereas, the AMO21c/T7c co-micelles at ratios of 1:3, 1:20, and 1:30 were larger than 300 nm. Those sizes are not favorable for intranasal delivery, which requires particles smaller than 200 nm for efficient transportation *via* olfactory neurons [43–45]. The AMO21c/T7c micelles showed a good level of polydispersity in their hydrodynamic size distribution. The zeta potentials had a tendency of increase along with the amount of T7c (Fig. 3E). The positive charge of the T7 peptide could contribute to that tendency.

The CMCs of AMO21c, T7c, and AMO21c/T7c were measured using DPH assays. The results indicate that AMO21c could not form micelles, even at 2.5 mg/ml (Fig. 4A), possibly because the repulsion of the negatively charged phosphate backbone dominated the hydrophobic interaction. The CMC of T7c was 0.045 mg/ml (Fig. 4B), and the CMC of the AMO21c/T7c co-micelles was 0.046 and 0.46 mg/ml for AMO21c and T7c, respectively (Fig. 4C).

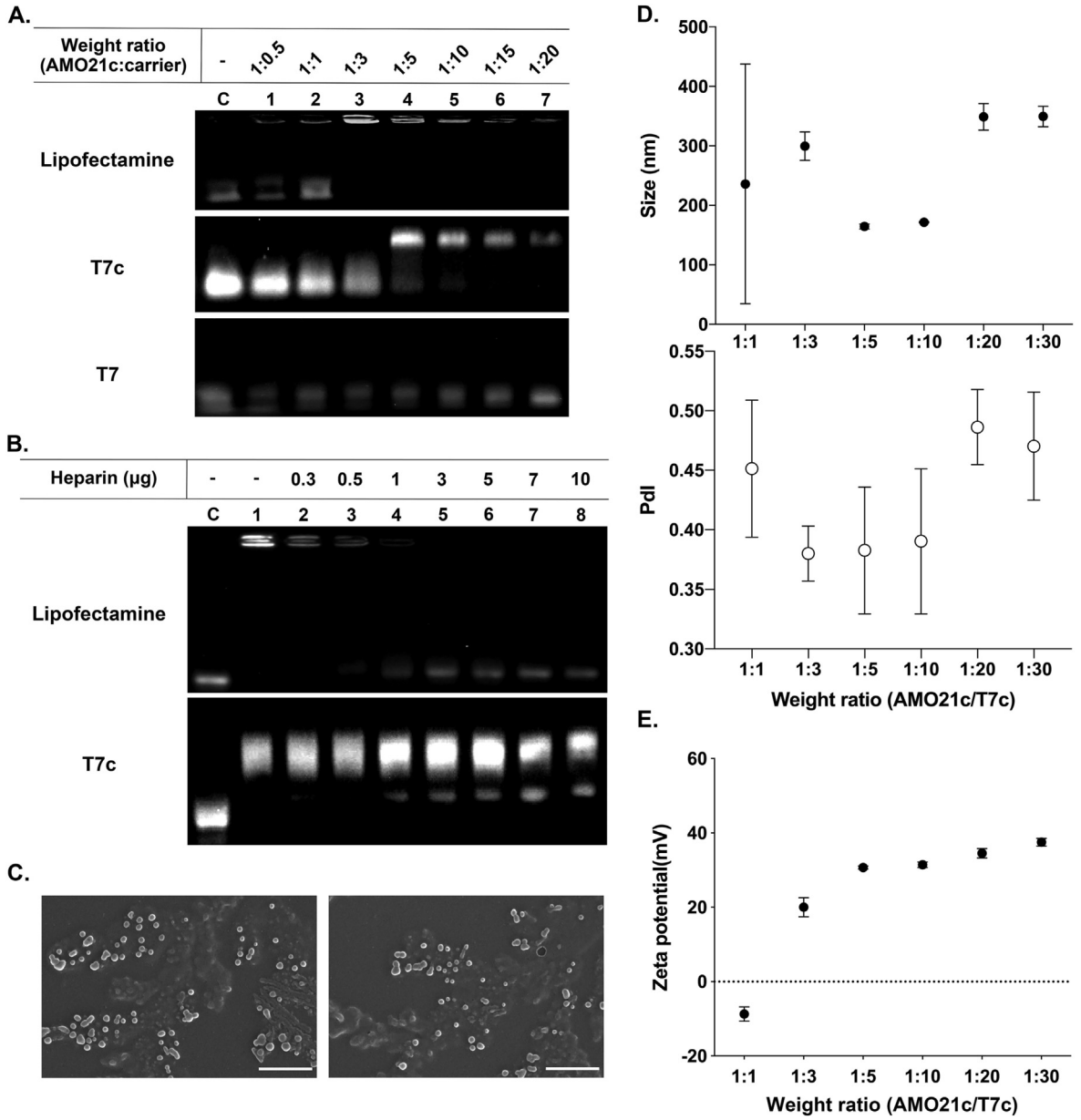


**Fig. 3. Physical characterization of the AMO21c/T7c co-micelles. (A) Gel retardation assay.** AMO21c was mixed with various amounts of carriers and analyzed on a 2% agarose gel. **(B) Heparin competition assay.** The AMO21c/T7c co-micelles were prepared at a 1:10 wt ratio. The AMO21c/lipofectamine complex was prepared at a 1:3 (w/v) ratio. Various amounts of heparin were added to the mixtures, and the samples were analyzed on a 2% agarose gel. **(C) SEM image.** The AMO21c/T7c co-micelles were prepared at a 1:10 wt ratio. The morphology was investigated by SEM. The scale bar indicates 500 nm. **(D) Particle size with its polydispersity (PDI)** and **(E) Zeta potential.** The sizes and zeta potentials of AMO21c/T7c co-micelles were measured by a zeta-sizer. The data are expressed as the mean ± standard deviation of triplicate experiments.

*Evaluation of transfection efficiency and cytotoxicity*

To test the delivery efficiency of the AMO21c/T7c mixed micelles, Cy5-AMO21c was delivered to C6 cells and measured by flow cytometry. Naked AMO21c and the AMO21c/lipofectamine complexes were used as controls. The AMO21c/T7c co-micelles had higher uptake efficiency than the naked AMO21c and AMO21c/lipofectamine complexes (Fig. 5A). This result was confirmed by fluorescence microscopy (Fig. 5B). The results show that the Cy5-positive signals in the AMO21c/T7c-treated cells were more intense than in those in the naked AMO21c and AMO21c/lipofectamine complexes (Fig. 5B). To identify TfR-mediated endocytosis mechanism by T7c, the Cy5-AMO21c delivery efficiency was measured to a less TfR expression cell line, HEK 293 cells, by flow cytometry. The results showed that there was no significant difference in Cy5-positive signals between AMO21c/Lipofectamine, AMO21c/T7c, and AMO21c/scrT7c groups (Supplementary Fig. 1). The results suggested that the T7 peptides was not able to mediate endocytosis, since there were not enough TfRs on the HEK 293 cell surface.

Cytotoxicity is another important factor in being able to apply the micelles for therapeutic purposes. Therefore, toxicity was measured using the 3-(4,5-Dimethylthiazol-2-yl)-2,5-diphenyltetrazolium bromide (MTT) assay in C6 cells. AMO21c has an anti-tumor effect, which might change the survival rate of tumor cells. Therefore, scrAMO21c was used for the MTT assay to evaluate the toxicity of the carriers (T7c and lipofectamine). Naked scrAMO21c, scrAMO21c/T7c co-micelles, and scrAMO21c/lipofectamine complexes were added to C6 cells at various doses of scrAMO21c. The viability of the cells was measured using MTT assays. In the

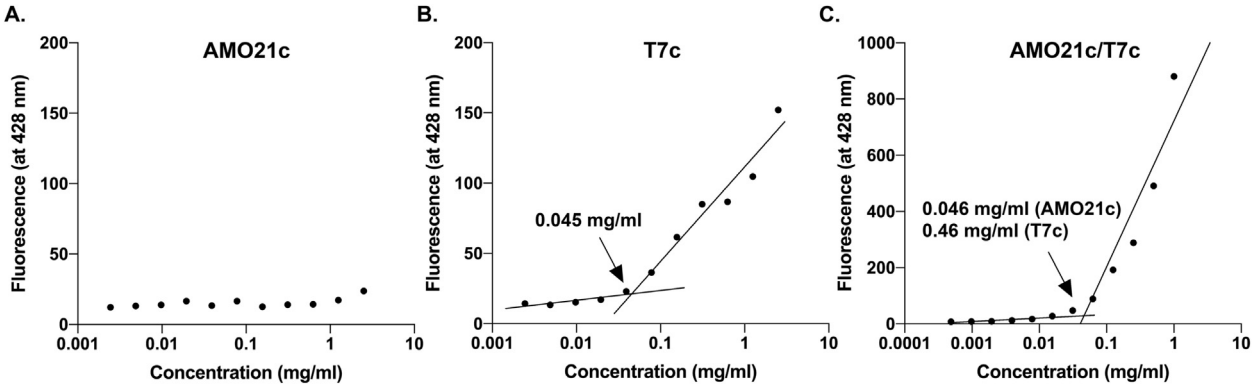


**Fig. 4. CMC.** The CMCs of **(A) AMO21c, (B) T7c,** and **(C) AMO21c/T7c** were measured by the DPH method.

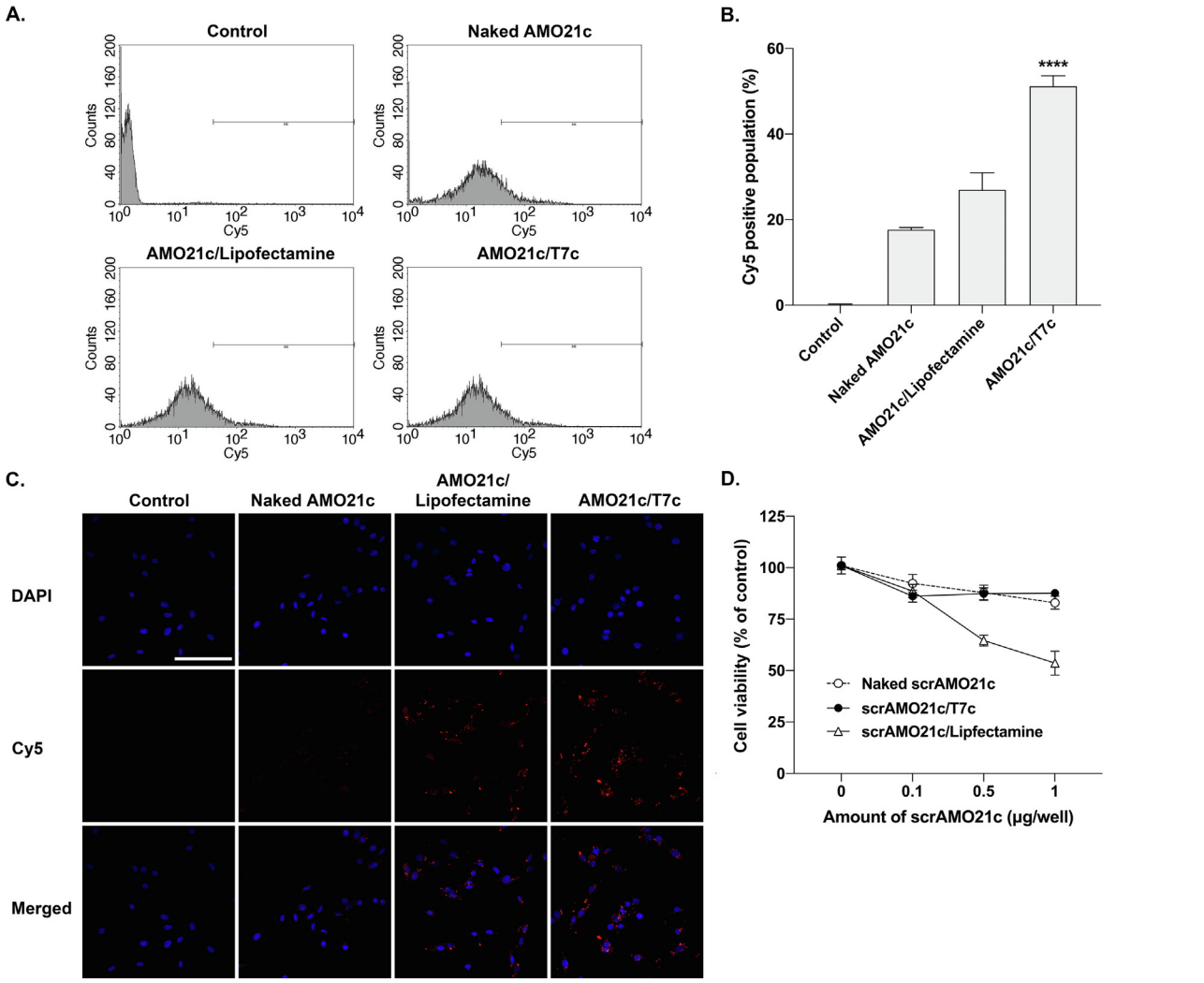


**Fig. 5. Comparison of delivery efficiency and cytotoxicity. (A) Fluorescence intensity histograms of flowcytometry and (B) Mean values of intracellular uptakes.** Naked Cy5-AMO21c, Cy5-AMO21c/lipofectamine, and Cy5-AMO21c/T7c were transfected into C6 cells. Cellular uptake was measured by flow cytometry. The data are expressed as the mean ± standard deviation of quadruplicate experiments. ****P < 0.0001 compared with the other samples. **(C) Fluorescence microscopy.** Delivery efficiency was measured by fluorescence microscopy. **(D) MTT assay.** Naked scrAMO21c, scrAMO21c/lipofectamine, and scrAMO21c/T7c were transfected into C6 cells. The cytotoxicity of the samples was measured using the MTT assay. The data are expressed as the mean ± standard deviation of octuplicate experiments.

range of doses tested (0.1–1 μg/well), the scrAMO21c/lipofectamine complexes had higher toxicity than naked scrAMO21c or the scrAMO21c/T7c co-micelles (Fig. 5C), and the toxicity of naked scrAMO21c and the scrAMO21c/T7c co-micelles did not differ significantly from each other, suggesting that T7c has no significant toxicity to C6 cells.

*In vivo* toxicity of the AMO21c/T7c co-micelles was evaluated in the normal brain tissues of animal models after intranasal admin-

istration. Naked AMO21c, AMO21c/Lipofectamine complex, and scrAMO21c/T7c co-micelles were used as controls. TUNEL assay showed that the co-micelles did not induce apoptosis in the normal brain tissues (Supplementary Fig. 2A). In addition, the normal brain tissues were subjected to hematoxylin & eosin staining. The results indicated that there were no remarkable damages or inflammations in the normal brain samples (Supplementary Fig. 2B). The results suggest that the co-micelles did not induce cytotoxicity in the animal models after intranasal administration.

*Delivery of the AMO21c/T7c co-micelles to the intracranial glioblastoma model rats*

C6 cells were transplanted into the brains of rats to produce orthotopic glioblastoma models. One week after implantation, the Cy5.5-AMO21c/T7c co-micelles were intranasally administered to the intracranial glioblastoma model animals to evaluate delivery efficiency. To evaluate the targeting effect of the T7 peptide in the micelles, cholesterol-conjugated scrambled T7 peptides (scrT7c) were used to prepare mixed micelles with Cy5.5-AMO21c as a control. The results show that the naked AMO21c and AMO21c/scrT7c micelles had similar fluorescence signal intensities in the brain, and the AMO21c/T7c co-micelles produced a higher fluorescence signal (Fig. 6A). The quantitation of the fluorescence signals confirmed those results (Fig. 6B), which might reflect the effect of the T7 peptide, which increased binding to the cells via TfRs on the cell surfaces.

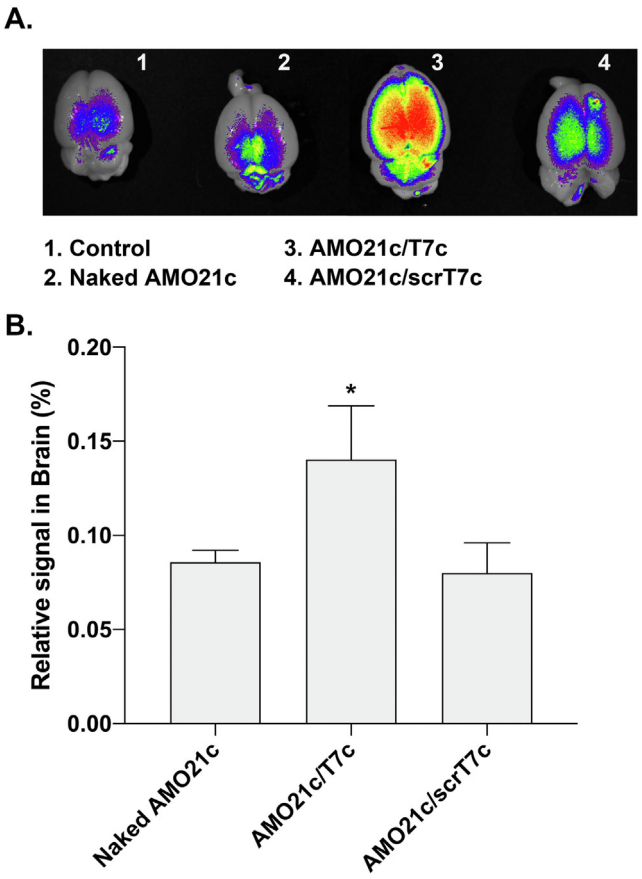


**Fig. 6. Delivery efficiency into the brain after intranasal administration.** Naked Cy5.5-AMO21c, Cy5.5-AMO21c/T7c, and Cy5.5-AMO21c/scrT7c were intranasally administered to the glioblastoma model rats. **(A) Brain images.** The brains were harvested and observed in an imaging box. **(B) Quantitation of positive signals.** The positive signals were quantitated. The data are expressed as the mean ± standard deviation of triplicate experiments. *P < 0.05 compared with the other samples.

*Evaluation of the therapeutic effects of the AMO21c/T7c co-micelles*

To evaluate the therapeutic effects of the AMO21c/T7c co-micelles, the micelles were administered intranasally three times to the intracranial glioblastoma model animals by using a POD. Naked AMO21c, AMO21c/lipofectamine, AMO21c/T7c, and scrAMO21c/T7c co-micelles were instilled into the model animals by intranasal administration. One week after administration, the brains were analyzed by various methods. The anti-miR-21 effect was evaluated by RT-PCR from the brain tissues. Those results indicate that the miR-21 level in the AMO21c/T7c group was significantly lower than in the AMO21c/lipofectamine and scrAMO21c/T7c groups (Fig. 7). The greater reduction produced by the AMO21c/T7c co-micelles, compared with the AMO21c/lipofectamine complexes, might be due to their higher delivery efficiency, as shown in Fig. 6. In addition, the comparison between AMO21c and scrAMO21c suggests that the sequence of AMO21c was useful for inhibiting miR-21.

miR-21 is involved in PDCD4 and PTEN, which are involved in apoptosis and cell-growth inhibition. In glioblastoma, the induction of miR-21 decreases the expression of PDCD4 and PTEN, which increases tumor cell survival. Therefore, miR-21 inhibition by delivering AMO21c could increase the expression of PDCD4 and PTEN. To evaluate that effect, tumor tissues were immunostained with anti-PDCD4 antibodies. The results show that PDCD4 expression was induced most efficiently by the delivery of AMO21c/T7c co-micelles (Fig. 8A). The quantitation of positive signals indicates that significantly more PDCD4 was induced by the AMO21c/T7c co-micelles than by the other samples (Fig. 8B). Similarly, tumor tissues were stained with anti-PTEN antibodies, and those results confirm that PTEN was induced by the delivery of the AMO21c/

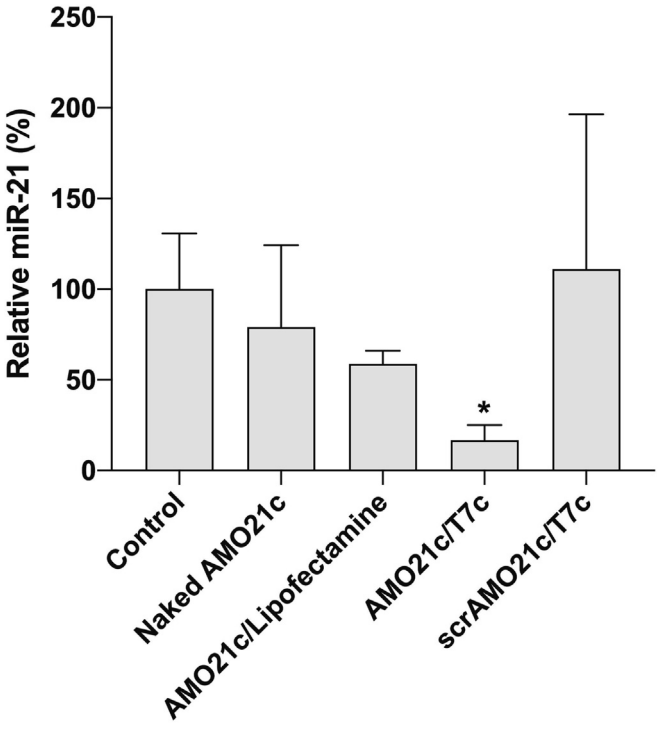


**Fig. 7. Suppression of miR-21 by delivering AMO21c/T7c co-micelles to glioblastoma.** Naked AMO21c, AMO21c/lipofectamine, AMO21c/T7c, and scrAMO21c/T7c were administered to the intracranial glioblastoma model animals by intranasal instillation. After 7 days, the brains were harvested, and total RNA was extracted from the tumor tissues. miR-21 was amplified by RT-PCR. The data are expressed as the mean ± standard deviation of quadruplicate experiments. *P < 0.05 compared with the control and scrAMO21c/T7c.

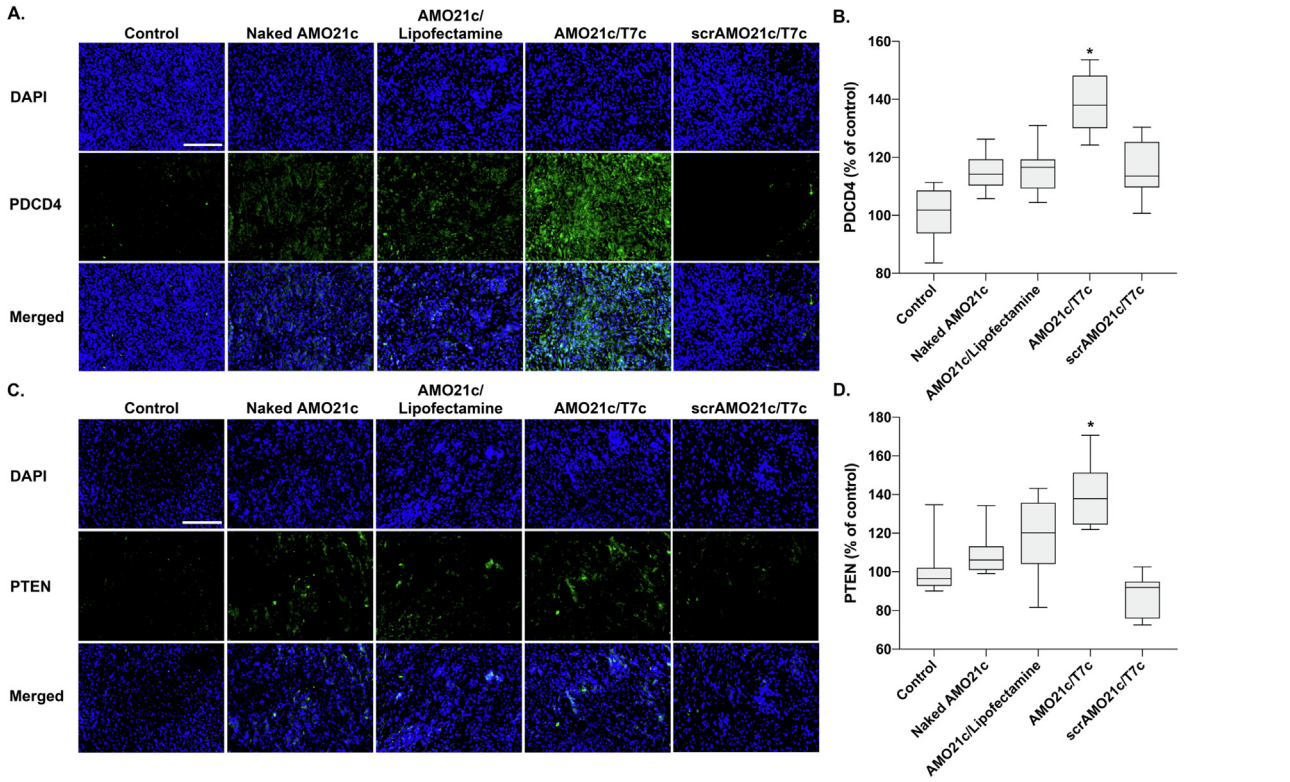


**Fig. 8. Immunohistochemistry for PDCD4 and PTEN.** Naked AMO21c, AMO21c/lipofectamine, AMO21c/T7c, and scrAMO21c/T7c were administered to the intracranial glioblastoma model animals by intranasal instillation. After 7 days, the brains were harvested and analyzed by immunostaining. **(A) Immunostaining of PDCD4, (B) quantitation of PDCD4 immunostaining, (C) immunostaining of PTEN, (D) quantitation of PTEN immunostaining.** Scale bar indicates 100 μm. The quantitation data are expressed as the mean ± standard deviation (n = 10).

T7c co-micelles (Fig. 8C and 8D). Thus, the reduction of miR-21 caused by the delivery of AMO21c increased the expression of PDCD4 and PTEN in the tumor tissues, which is closely related to cell growth inhibition and apoptosis. To evaluate those levels, Ki67 and TUNEL assays were performed with the tumor tissues. Several studies have indicated that the expression of the proliferation marker Ki67 is strongly proportional to cancer severity [46,47]. The Ki67 assay results in this study confirm that the proliferation of tumor cells was significantly inhibited in the AMO21c/T7c group, compared with the other groups (Fig. 9A). The quantitation analysis of the images confirmed that the Ki67 positive signals were decreased significantly in the AMO21c/T7c co-micelle group, compared with the other groups (Fig. 9B). Similarly, the apoptosis level was higher in the AMO21c/T7c groups than in the control and other sample groups (Fig. 9A). The quantitation analysis also indicated that the apoptosis level was significantly induced by the AMO21c/T7c co-micelles, compared to the other samples. (Fig. 9C).

The tumor sizes in each group were evaluated by Nissl staining. Naked AMO21c and the AMO21c/lipofectamine complexes reduced the tumor size compared with the control, but the difference was not statistically significant. However, the delivery of the AMO21c/T7c co-micelles significantly decreased the tumor size compared with the other groups (Fig. 10).

## Conclusion

In this study, T7c/AMO21c co-micelles were developed as a system for delivering AMO21 into the brain to treat glioblastoma. The co-micelles were evaluated in glioblastoma models after intranasal administration. Compared with control delivery systems (naked AMO21c and AMO21c/lipofectamine complexes), the AMO21c/T7c co-micelles had higher delivery efficiency of AMO21 into the brain. As a result, the tumor size was decreased more effectively by intranasal administration of AMO21c/T7c co-micelles than by naked AMO21c, AMO21c/lipofectamine, or scrAMO21c/T7c. The results suggest that intranasal administration of mixed micelles of AMO21c and T7c could efficiently deliver AMO21 into brain tumors. Although the results showed an advanced system for gene therapy to treat glioblastoma, in-depth studies regarding optimal administration doses and real-time pharmacokinetics are required for clinical application.

## CRediT authorship contribution statement

**Youngki Lee:** Investigation, Methodology, Formal analysis, Data curation, Writing – original draft. **Junkyu Ha:** Investigation, Methodology, Formal analysis, Data curation, Writing – original draft. **Minkyung Kim:** Investigation. **Subin Kang:** Investigation. **Minji Kang:** Investigation. **Minhyung Lee:** Conceptualization, Methodology, Formal analysis, Data curation, Writing – review & editing, Supervision, Funding acquisition.

## Data Availability

The data that support the findings of this study are available from the corresponding author upon reasonable request.

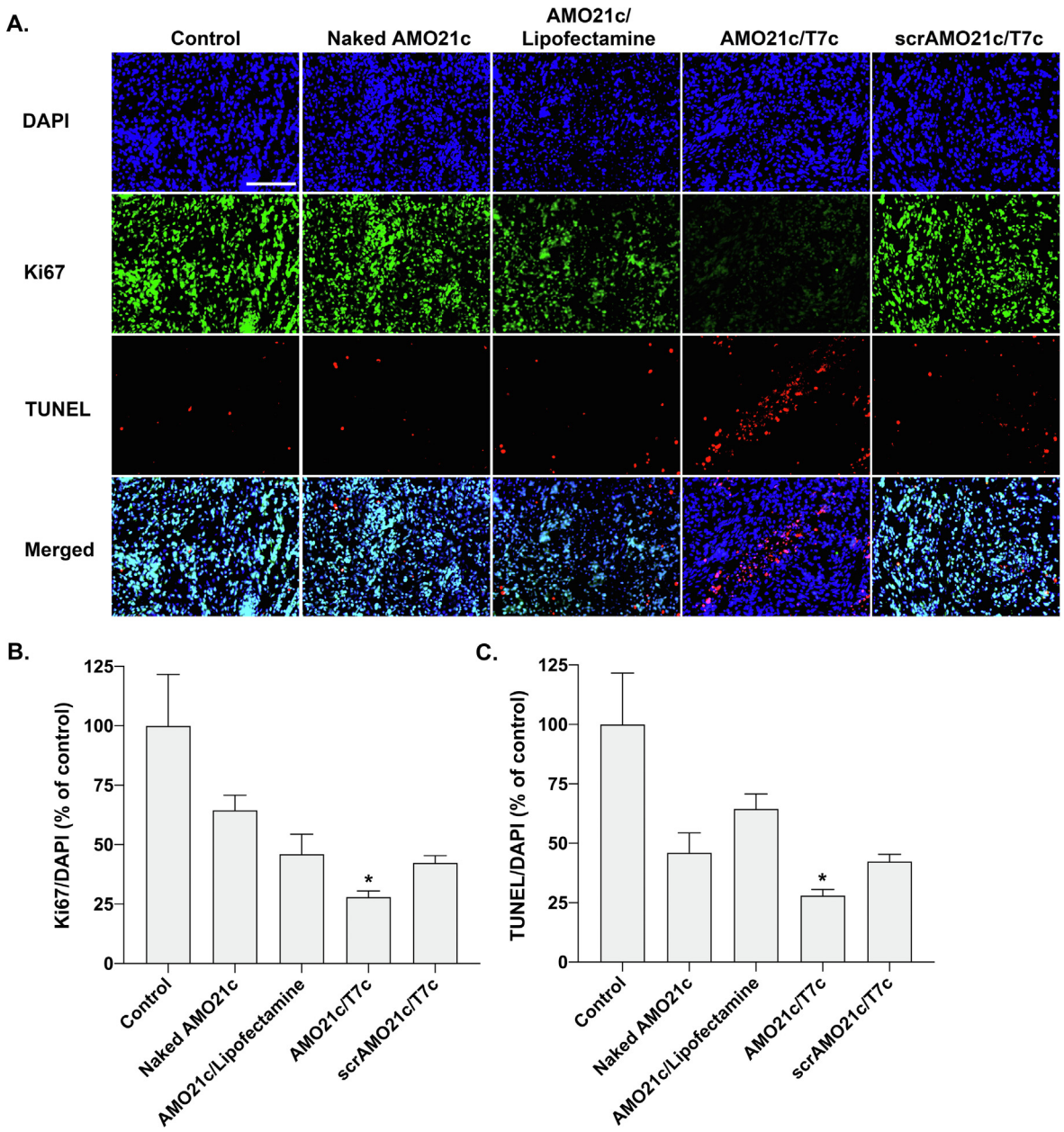


**Fig. 9. Proliferation and apoptosis assays.** Naked AMO21c, AMO21c/lipofectamine, AMO21c/T7c, and scrAMO21c/T7c were administered to the intracranial glioblastoma model animals by intranasal instillation. After 7 days, the brains were harvested and analyzed by **(A) Immunostaining of Ki67 and TUNEL assays, (B) Quantitation of the Ki67 levels, (C) Quantiation of the TUNEL signals**. The quantitation of the Ki67 and TUNEL levels was measured by Zeiss Zen software. The data are expressed as mean value ± standard deviation (n = 8). *P < 0.05 as compared with the other groups. Scale bar indicates 100 μm.

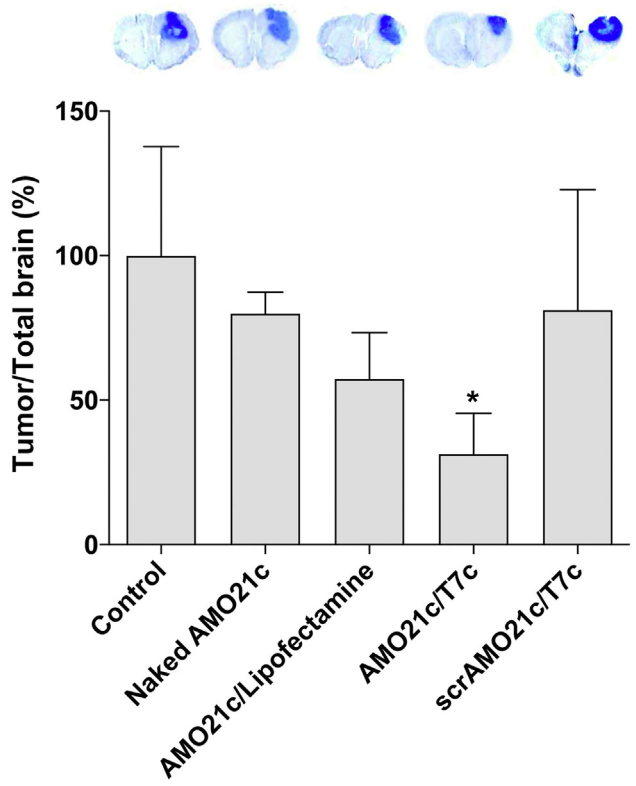


**Fig. 10. Tumor size.** Naked AMO21c, AMO21c/lipofectamine, AMO21c/T7c, and scrAMO21c/T7c were administered to the intracranial glioblastoma model animals by intranasal instillation. After 7 days, the brains were harvested and analyzed by Nissl staining. The relative tumor sizes are presented as % of the control group. The data are expressed as the mean ± standard deviation of quintuplicate experiments. *P < 0.05 compared with the control, naked AMO21c, and scrAMO21c/T7c.

## Declaration of Competing Interest

The authors declare that they have no known competing financial interests or personal relationships that could have appeared to influence the work reported in this paper.

## Acknowledgement

This work was supported by the Individual Basic Science & Engineering Research Program (2022R1A2B5B01001920) through the National Research Foundation, funded by the Ministry of Science and ICT in Korea.

## Appendix A. Supplementary material

Supplementary data to this article can be found online at https://doi.org/10.1016/j.jare.2023.01.005.

## References

[1] Tait MJ, Petrik V, Loosemore A, Bell BA, Papadopoulos MC. Survival of patients with glioblastoma multiforme has not improved between 1993 and 2004: analysis of 625 cases. Br J Neurosurg 2007;21:496–500. doi: https://doi.org/10.1080/02688690701449251.

[2] Adamson C, Kanu OO, Mehta AI, Di C, Lin N, Mattox AK, et al. Glioblastoma multiforme: a review of where we have been and where we are going. Expert Opin Investig Drugs 2009;18:1061–83. doi: https://doi.org/10.1517/13543780903052764.

[3] Furnari FB, Fenton T, Bachoo RM, Mukasa A, Stommel JM, Stegh A, et al. Malignant astrocytic glioma: genetics, biology, and paths to treatment. Genes Dev 2007;21:2683–710. doi: https://doi.org/10.1101/gad.1596707.

[4] Seystahl K, Wick W, Weller M. Therapeutic options in recurrent glioblastoma–An update. Crit Rev Oncol Hematol 2016;99:389–408. doi: https://doi.org/10.1016/j.critrevonc.2016.01.018.

[5] Corsten MF, Miranda R, Kasmieh R, Krichevsky AM, Weissleder R, Shah K. MicroRNA-21 knockdown disrupts glioma growth in vivo and displays synergistic cytotoxicity with neural precursor cell delivered S-TRAIL in human gliomas. Cancer Res 2007;67:8994–9000. doi: https://doi.org/10.1158/0008-5472.CAN-07-1045.

[6] Kwiatkowska A, Nandhu MS, Behera P, Chiocca EA, Viapiano MS. Strategies in gene therapy for glioblastoma. Cancers (Basel) 2013;5:1271–305. doi: https://doi.org/10.3390/cancers5041271.

[7] Alemany R, Gomez-Manzano C, Balague C, Yung WK, Curiel DT, Kyritsis AP, et al. Gene therapy for gliomas: molecular targets, adenoviral vectors, and oncolytic adenoviruses. Exp Cell Res 1999;252:1–12. doi: https://doi.org/10.1006/excr.1999.4623.

[8] Mirzaei S, Mahabady MK, Zabolian A, Abbaspour A, Fallahzadeh P, Noori M, et al. Small interfering RNA (siRNA) to target genes and molecular pathways in glioblastoma therapy: Current status with an emphasis on delivery systems. Life Sci 2021;275:. doi: https://doi.org/10.1016/j.lfs.2021.119368119368.

[9] Song H, Oh B, Choi M, Oh J, Lee M. Delivery of anti-microRNA-21 antisense-oligodeoxynucleotide using amphiphilic peptides for glioblastoma gene therapy. J Drug Target 2015;23:360–70. doi: https://doi.org/10.3109/1061186X.2014.1000336.

[10] Yang ZZ, Li JQ, Wang ZZ, Dong DW, Qi XR. Tumor-targeting dual peptides-modified cationic liposomes for delivery of siRNA and docetaxel to gliomas. Biomaterials 2014;35:5226–39. doi: https://doi.org/10.1016/j.biomaterials.2014.03.017.

[11] Stenvang J, Petri A, Lindow M, Obad S, Kauppinen S. Inhibition of microRNA function by antimiR oligonucleotides. Silence 2012;3:1. doi: https://doi.org/10.1186/1758-907X-3-1.

[12] Costa PM, Cardoso AL, Custodia C, Cunha P, Pereira de Almeida L, Pedroso de Lima MC. MiRNA-21 silencing mediated by tumor-targeted nanoparticles combined with sunitinib: a new multimodal gene therapy approach for glioblastoma. J Control Release 2015;207:31–9. doi: https://doi.org/10.1016/j.jconrel.2015.04.002.

[13] Kim G, Kim M, Lee Y, Byun JW, Hwang DW, Lee M. Systemic delivery of microRNA-21 antisense oligonucleotides to the brain using T7-peptide decorated exosomes. J Control Release 2020;317:273–81. doi: https://doi.org/10.1016/j.jconrel.2019.11.009.

[14] Zhuang C, Piao C, Choi M, Ha J, Lee M. Delivery of miRNA-92a inhibitor using RP1-linked peptide elicits anti-inflammatory effects in an acute lung injury model. J Biomed Nanotechnol 2021;17:1273–83. doi: https://doi.org/10.1166/jbn.2021.3102.

[15] Krutzfeldt J, Rajewsky N, Braich R, Rajeev KG, Tuschl T, Manoharan M, et al. Silencing of microRNAs in vivo with 'antagomirs'. Nature 2005;438:685–9. doi: https://doi.org/10.1038/nature04303.

[16] Stratton MR, Campbell PJ, Futreal PA. The cancer genome. Nature 2009;458:719–24. doi: https://doi.org/10.1038/nature07943.

[17] Chen Y, Liu W, Chao T, Zhang Y, Yan X, Gong Y, et al. MicroRNA-21 down-regulates the expression of tumor suppressor PDCD4 in human glioblastoma cell T98G. Cancer Lett 2008;272:197–205. doi: https://doi.org/10.1016/j.canlet.2008.06.034.

[18] Croce CM. Causes and consequences of microRNA dysregulation in cancer. Nat Rev Genet 2009;10:704–14. doi: https://doi.org/10.1038/nrg2634.

[19] Meng F, Henson R, Wehbe-Janek H, Ghoshal K, Jacob ST, Patel T. MicroRNA-21 regulates expression of the PTEN tumor suppressor gene in human hepatocellular cancer. Gastroenterol 2007;133:647–58. doi: https://doi.org/10.1053/j.gastro.2007.05.022.

[20] Ha J, Kim M, Lee Y, Lee M. Intranasal delivery of self-assembled nanoparticles of therapeutic peptides and antagomirs elicits anti-tumor effects in an intracranial glioblastoma model. Nanoscale 2021;13:14745–59. doi: https://doi.org/10.1039/d1nr03455c.

[21] Oh B, Song H, Lee D, Oh J, Kim G, Ihm SH, et al. Anti-cancer effect of R3V6 peptide-mediated delivery of an anti-microRNA-21 antisense-oligodeoxynucleotide in a glioblastoma animal model. J Drug Target 2017;25:132–9. doi: https://doi.org/10.1080/1061186X.2016.1207648.

[22] Tan X, Kim G, Lee D, Oh J, Kim M, Piao C, et al. A curcumin-loaded polymeric micelle as a carrier of a microRNA-21 antisense-oligonucleotide for enhanced anti-tumor effects in a glioblastoma animal model. Biomater Sci 2018;6:407–17. doi: https://doi.org/10.1039/c7bm01088e.

[23] Wang H, Ding S, Zhang Z, Wang L, You Y. Cationic micelle: A promising nanocarrier for gene delivery with high transfection efficiency. J Gene Med 2019;21:e3101.

[24] Kang HC, Huh KM, Bae YH. Polymeric nucleic acid carriers: current issues and novel design approaches. J Control Release 2012;164:256–64. doi: https://doi.org/10.1016/j.jconrel.2012.06.036.

[25] Li SD, Huang L. Gene therapy progress and prospects: non-viral gene therapy by systemic delivery. Gene Ther 2006;13:1313–9. doi: https://doi.org/10.1038/sj.gt.3302838.

[26] Zhang Y, Chan HF, Leong KW. Advanced materials and processing for drug delivery: the past and the future. Adv Drug Deliv Rev 2013;65:104–20. doi: https://doi.org/10.1016/j.addr.2012.10.003.

[27] Fischer D, Bieber T, Li Y, Elsasser HP, Kissel T. A novel non-viral vector for DNA delivery based on low molecular weight, branched polyethylenimine: effect of molecular weight on transfection efficiency and cytotoxicity. Pharm Res 1999;16:1273–9. doi: https://doi.org/10.1023/a:1014861900478.

[28] Choi M, Thuy LT, Lee Y, Piao C, Choi JS, Lee M. Dual-Functional Dendrimer Micelles with Glycyrrhizic Acid for Anti-Inflammatory Therapy of Acute Lung Injury. ACS Appl Mater Interfaces 2021;13:47313–26. doi: https://doi.org/10.1021/acsami.1c08107.
[29] Piao C, Park JH, Lee M. Anti-Inflammatory therapeutic effect of adiponectin gene delivery using a polymeric carrier in an acute lung injury model. Pharm Res 2017;34:1517–26. doi: https://doi.org/10.1007/s11095-017-2175-6.
[30] Kim G, Piao C, Oh J, Lee M. Combined delivery of curcumin and the heme oxygenase-1 gene using cholesterol-conjugated polyamidoamine for anti-inflammatory therapy in acute lung injury. Phytomedicine 2019;56:165–74. doi: https://doi.org/10.1016/j.phymed.2018.09.240.
[31] Haraszti RA, Miller R, Didiot MC, Biscans A, Alterman JF, Hassler MR, et al. Optimized cholesterol-siRNA chemistry improves productive loading onto extracellular vesicles. Mol Ther 2018;26:1973–82. doi: https://doi.org/10.1016/j.ymthe.2018.05.024.
[32] Lochhead JJ, Thorne RG. Intranasal delivery of biologics to the central nervous system. Adv Drug Deliv Rev 2012;64:614–28. doi: https://doi.org/10.1016/j.addr.2011.11.002.
[33] Kim M, Lee Y, Lee M. Hypoxia-specific anti-RAGE exosomes for nose-to-brain delivery of anti-miR-181a oligonucleotide in an ischemic stroke model. Nanoscale 2021;13:14166–78. doi: https://doi.org/10.1039/d0nr07516g.
[34] Sabir F, Ismail R, Csoka I. Nose-to-brain delivery of antiglioblastoma drugs embedded into lipid nanocarrier systems: status quo and outlook. Drug Discov Today 2020;25:185–94. doi: https://doi.org/10.1016/j.drudis.2019.10.005.
[35] Sun X, Wang G, Zhang H, Hu S, Liu X, Tang J, et al. The blood clearance kinetics and pathway of polymeric micelles in cancer drug delivery. ACS Nano 2018;12:6179–92. doi: https://doi.org/10.1021/acsnano.8b02830.
[36] Kim S, Shi Y, Kim JY, Park K, Cheng JX. Overcoming the barriers in micellar drug delivery: loading efficiency, in vivo stability, and micelle-cell interaction. Expert Opin Drug Deliv 2010;7:49–62. doi: https://doi.org/10.1517/17425240903380446.
[37] Takeda KM, Yamasaki Y, Dirisala A, Ikeda S, Tockary TA, Toh K, et al. Effect of shear stress on structure and function of polyplex micelles from poly(ethylene glycol)-poly(l-lysine) block copolymers as systemic gene delivery carrier. Biomaterials 2017;126:31–8. doi: https://doi.org/10.1016/j.biomaterials.2017.02.012.
[38] Aliabadi HM, Shahin M, Brocks DR, Lavasanifar A. Disposition of drugs in block copolymer micelle delivery systems: from discovery to recovery. Clin Pharmacokinet 2008;47:619–34. doi: https://doi.org/10.2165/00003088-200847100-00001.
[39] Han LA, Huang RQ, Liu SH, Huang SX, Jiang C. Peptide-conjugated PAMAM for targeted doxorubicin delivery to transferrin receptor overexpressed tumors. Mol Pharm 2010;7:2156-65. https://doi.org/doi.org/10.1021/mp100185f.
[40] Chirasani SR, Markovic DS, Synowitz M, Eichler SA, Wisniewski P, Kaminska B, et al. Transferrin-receptor-mediated iron accumulation controls proliferation and glutamate release in glioma cells. J Mol Med (Berl) 2009;87:153–67. doi: https://doi.org/10.1007/s00109-008-0414-3.
[41] Kim M, Oh J, Lee Y, Lee EH, Ko SH, Jeong JH, et al. Delivery of self-replicating messenger RNA into the brain for the treatment of ischemic stroke. J Control Release 2022;350:471–85. doi: https://doi.org/10.1016/j.jconrel.2022.08.049.
[42] Ullah I, Chung K, Oh J, Beloor J, Bae S, Lee SC, et al. Intranasal delivery of a Fas-blocking peptide attenuates Fas-mediated apoptosis in brain ischemia. Sci Rep 2018;8:15041. doi: https://doi.org/10.1038/s41598-018-33296-z.
[43] Costa CP, Moreira JN, Sousa Lobo JM, Silva AC. Intranasal delivery of nanostructured lipid carriers, solid lipid nanoparticles and nanoemulsions: A current overview of in vivo studies. Acta Pharm Sin B 2021;11:925–40. doi: https://doi.org/10.1016/j.apsb.2021.02.012.
[44] Muntimadugu E, Dhommati R, Jain A, Challa VG, Shaheen M, Khan W. Intranasal delivery of nanoparticle encapsulated tarenflurbil: A potential brain targeting strategy for Alzheimer's disease. Eur J Pharm Sci 2016;92:224–34. doi: https://doi.org/10.1016/j.ejps.2016.05.012.
[45] Su Y, Sun B, Gao X, Dong X, Fu L, Zhang Y, et al. Intranasal delivery of targeted nanoparticles loaded with miR-132 to brain for the treatment of neurodegenerative diseases. Front Pharmacol 2020;11:1165. doi: https://doi.org/10.3389/fphar.2020.01165.
[46] Chen WJ, He DS, Tang RX, Ren FH, Chen G. Ki-67 is a valuable prognostic factor in gliomas: evidence from a systematic review and meta-analysis. Asian Pac J Cancer Prev 2015;16:411–20. doi: https://doi.org/10.7314/apjcp.2015.16.2.411.
[47] Stathopoulos GP, Malamos NA, Markopoulos C, Polychronis A, Armakolas A, Rigatos S, et al. The role of Ki-67 in the proliferation and prognosis of breast cancer molecular classification subtypes. Anticancer Drugs 2014;25:950–7. doi: https://doi.org/10.1097/CAD.0000000000000123.